12th International Conference on Fracture Mechanics of Concrete and Concrete Structures
FraMCoS-12
B.L.A. Pichler, Ch. Hellmich, P. Preinstorfer (Eds)

https://doi.org/10.21012/FC12.1174
MS01-2:2

INFLUENCE OF TENSILE SOFTENING PROPERTIES ON SHEAR BEHAVIOR OF R/FRC BEAMS

NAOSHI UEDA[*], YUTA NAKAMICHI[†]

[*] Kansai University, Department of Civil, Environmental and Applied Systems Engineering
3-3-35, Yamate-cho, Suita, Osaka, Japan
e-mail: n.ueda@kansai-u.ac.jp

[†] Hanshin Expressway Co., Ltd.
3-2-4 Nakanoshima, Kita-ku, Osaka, Japan
e-mail: yuta-nakamichi@hanshin-exp.co.jp

Key words: Shear diagonal failure, Fracture energy, Fiber Reinforced Concrete with micro fiber

Abstract: Many researchers have evaluated the structural performance of R/FRC, which refers to fiber-reinforced concrete beams reinforced with rebars. While it is well known that fiber inclusion enhances the shear strength of R/FRC, a unified evaluation method has not yet been developed. This study conducted shear-flexural loading tests on R/FRC beams to understand the effect of tensile softening properties on their shear behavior, by both experiments and simulations. In the experiments, various FRCs with different tensile softening properties were produced by altering fiber types and contents, and the shear failure behavior of the R/FRC beams was observed up to failure. Additionally, the effect of tensile softening properties on shear behavior was investigated using 3D RBSM simulation. The results indicated that the flexural stiffness of R/FRC beams after cracking is influenced by the magnitude of tensile stress in the FRC post-cracking and that the shear strength strongly depends on the tensile softening behavior of the FRC. It was also confirmed that the shear strength could be estimated using the fracture energy of the FRC.

1 INTRODUCTION

Fiber-reinforced cement composites (FRCC), including both Fiber-reinforced Concrete (FRC) and Fiber-reinforced Mortar (FRM), are expected to be applied to structural components owing to their excellent tensile performance. However, reflecting the effects of fibers appropriately in the design code proves challenging. Numerous studies have been conducted to evaluate FRCC reinforced with steel bars (R/FRCC), particularly focusing on the shear strength of R/FRCC when applied to structural members. Although these studies show that fiber incorporation is effective in improving shear strength, most of them focus on specific types of FRCC, and no unified evaluation method for any FRCC has been established. As new FRCC materials are expected to be developed in the future, it is desirable to quantitatively assess the shear-strengthening effects of FRCC for their structural applications.

The authors have developed a FRC using microfibers, which are 12 mm in length and 0.04 mm in diameter, as a replacement for the conventional macrofibers, which are 30 mm in length and 0.66 mm in diameter. This material demonstrated that the stress drop immediately after crack initiation was reduced compared to conventional FRC. Additionally, in R/FRC members, materials that can maintain higher tensile stress after crack formation exhibit a greater tension stiffening effect[2]. Based on these results, it is believed that by focusing on

the tensile softening characteristics, the structural performance of R/FRC can be quantitatively evaluated.

In this paper, to understand the impact of tensile softening characteristics, such as fracture energy, on the shear behavior of R/FRC members, the shear failure behavior of R/FRC beams was investigated using both experimental and analytical approaches.

2 OUTLINE OF EXPERIMENT

2.1 Specimen dimensions and loading condition

Figure 1 shows the dimensions and reinforcement layout of the R/FRC beam. The beam has dimensions of 150 mm in width, 200 mm in height, and 1800 mm in length. Two D22 steel bars, with a yield strength (f_y) of 390 N/mm², were placed 165 mm from the upper edge of the section. The ends of the reinforcing bars were not mechanically anchored using bending or steel plates, instead, anchorage was achieved by providing a 300 mm development length outside the supports.

The load was applied at two points with a shear span of 500 mm and a constant moment span of 200 mm. The shear span ratio is 3.03, and in the case of no fiber inclusion, the beam was designed to fail in shear.

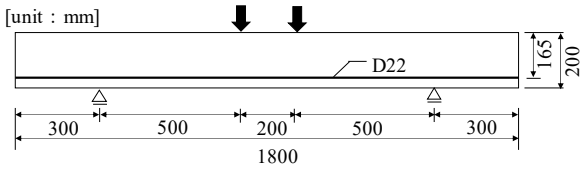

Figure 1: Beam specimen.

2.2 Mix proportion and curing condition

Table 1 shows the mix proportions of the FRCs used in this study. The water-to-binder ratio was set at 40%, and the binder consisted of cement and fly ash, with 30% of the cement replaced by fly ash. Fibers were incorporated by replacing fine aggregates, while the unit volume of coarse aggregates was kept constant. The fibers used were polyvinyl alcohol fibers (PVA), specifically PVA30 with a diameter of 660 μm and a length of 30 mm, and PVA12 with a diameter of 40 μm and a length of 12 mm.

The specimens were demolded one day after casting, cured under wet conditions by covering them with wet cloth, and loading tests were conducted at a material age of 35 days.

Table 1: Mix proportions

Case	Vf (%)	(kg/m³) W	C	FA	S	G
NC	-	200	350	150	757	751
PVA12-0.5	0.5				737	
PVA12-1.0	1.0				749	
PVA30-1.0						
PVA12-1.5	1.5	220	385	165	614	

2.3 Mechanical properties of FRCs

Table 2 shows the results of compressive strength (f'_c) and static elastic modulus (E_c) from cylindrical specimens. The compressive strength ranged from 47.2 N/mm² to 51.1 N/mm², and the static elastic modulus ranged from 28.9 N/mm² to 31.8 N/mm². No significant effects of fiber inclusion on the mechanical properties were observed.

Table 2: Material properties

Case	f'_c (N/mm²)	E_c (kN/mm²)
NC	50.8	31.8
PVA12-0.5	51.1	29.7
PVA12-1.0	50.7	30.6
PVA30-1.0	49.6	29.5
PVA12-1.5	49.8	30.3

Figure 2 shows the load-CMOD relationship obtained from a three-point bending test with a notch, and Figure 3 presents an example of the tension softening curve derived using the multiple linear approximation method [3]. The tension softening curves in the figure were obtained from the lower bound values of the load-CMOD relationships for each specimen. From the tension softening curves, it can be observed that PVA30-1.0 exhibits the characteristic of retaining stress even when cracks open to some extent. On the other hand, specimens with PVA12 fibers show a suppression of the stress drop immediately

after cracking, and this trend becomes more pronounced as the fiber content increases.

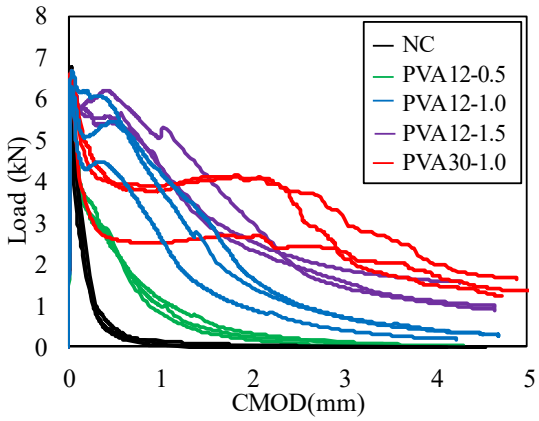

Figure 2: Load-CMOD relationships.

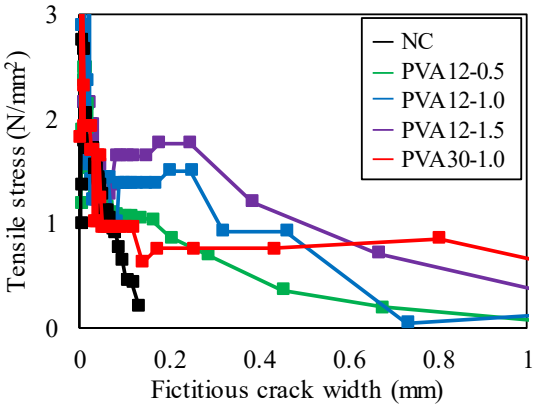

Figure 3: Tension softening curves.

3 OUTLINES OF ANALYSIS

3.1 Analytical method

In this study, 3D-RBSM analysis was conducted. For the constitutive law, the nonlinear model developed by Yamamoto et al. [4] was applied, where the compressive softening behavior due to vertical springs was not modeled, and concrete failure was represented by the tensile softening behavior of the vertical springs and the sliding behavior of the shear springs. Reinforcing bars were modeled using beam elements.

3.2 Analytical conditions

Figure 4 shows the mesh discretization of the beam used in the analysis. The element size was set to approximately 15 mm. The boundary conditions were the same as those in the experiment, with a shear span of 500 mm and a constant bending section of 200 mm, using a two-point loading configuration. The load was introduced by displacement control of the upper loading plate element. The displacement increment per step was set to 0.01 mm, and the convergence condition was set such that the ratio of the norm of the residual force to the norm of the applied load was less than 0.1%.

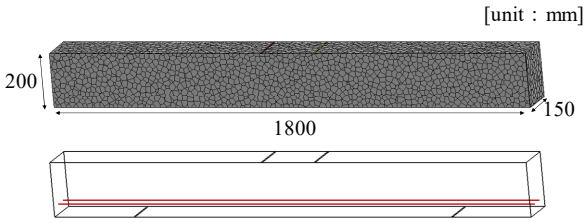

Figure 4: mesh discretization.

3.3 Identification of tension softening curves

In the analysis, it is important to model the tensile softening behavior of FRC. In this study, the tensile softening curves obtained in the previous chapter were modeled using a trilinear model for each FRC. Figure 5 shows the modeled tensile softening curves. Figure 6 presents the load-CMOD relationship obtained from a three-point bending test via analysis. The experimental load-CMOD relationships are also shown in the figure for comparison. From the figure, it can be confirmed that, for all FRCs, the extent of the load drop after crack initiation observed in the experiments is generally well reproduced.

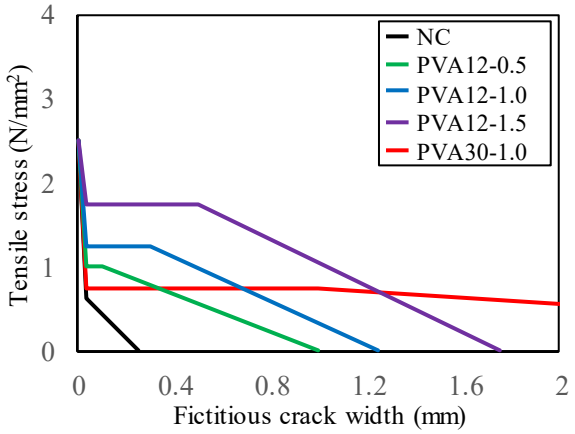

Figure 5: Modeling of tension softening curves.

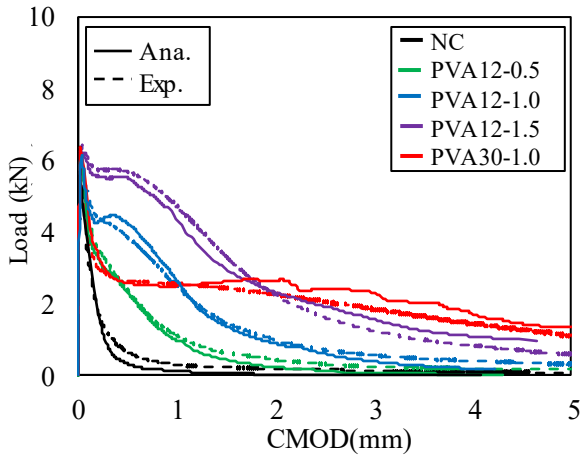

Figure 6: Comparison of load-CMOD relationships between analysis and experiment.

4 RESULTS AND DISCUSSION

4.1 Shear failure behavior

Figure 7 shows the load-displacement relationship obtained from the loading test. In the figure, the diagonal crack initiation load (2×Vc) calculated using Niwa's equation [5] and the ultimate bending load (Mu/250), derived from the ultimate bending moment, are also shown for comparison.

The NC specimen exhibited diagonal cracking at 95.2 kN, followed by a sudden drop in load leading to failure. In contrast, the FRC specimens, both the PVA30 and PVA12 specimens, were able to increase the load even beyond 100 kN. Focusing on bending stiffness, the PVA30 specimen showed a decrease in bending stiffness around 120 kN, whereas the PVA12 specimens showed no reduction in bending stiffness, regardless of the fiber content. This is likely because the FRC with PVA12 experienced a smaller reduction in tensile stress immediately after crack initiation compared to the FRC with PVA30 as mentioned in the previous chapter, which helped suppress the decrease in bending stiffness due to the opening of diagonal cracks.

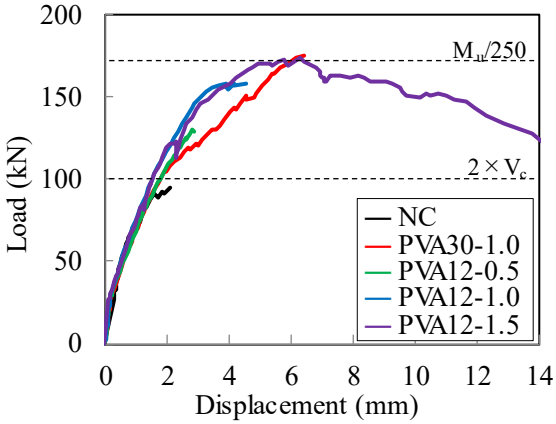

Figure 7: Load-displacement relationships (experiment).

Focusing on the failure behavior, all specimens except for the PVA12-1.5 specimen exhibited a sudden drop in load and failure due to the opening of diagonal cracks. Upon examining the crack surfaces after failure, fiber rupture was observed in all specimens. On the other hand, the PVA12-1.5 specimen exhibited a gradual decrease in load accompanied by deformation in the post-peak region. At a displacement of approximately 7 mm, it was confirmed that the reinforcing bars yielded, as measured by strain gauges attached to them. Figure 8 shows the appearance of the diagonal crack at a displacement of 10 mm for the PVA12-1.5 specimen. According to measurements using a crack scale, the widest diagonal crack opening was approximately 0.6 mm. This suggests that, even in the post-peak region, the crack opening was suppressed due to the bridging effect of the fibers. Based on these observations, it can be concluded that the failure behavior of the PVA12-1.5 specimen was different from that of the other specimens.

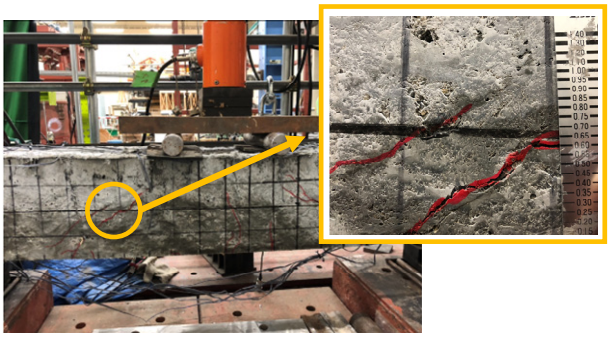

Figure 8: Diagonal crack of the PVA12-1.5 specimen.

Figure 9 shows the load-displacement relationship obtained from the analysis. Until the bending crack occurred at approximately 40 kN, no clear differences in behavior were observed among the specimens. For the NC specimen, the stiffness sharply decreased from around 75 kN, reaching the maximum load at 107 kN. In the analysis, the diagonal crack did not open and propagate immediately, resulting in a maximum load higher than that observed in the experiments.

For the FRC specimens, the maximum load was found to be higher than that of the NC specimen, as observed in the experiment. The maximum load of each specimen was generally similar to the experimental results.

Focusing on the stiffness after 80 kN, the PVA12-0.5 specimen showed a sharp decrease in stiffness around 110 kN. In contrast, for the PVA12-1.0 and PVA12-1.5 specimens, the stiffness was observed to be higher compared to the PVA30-1.0 specimen. From these results, it can be concluded that the bending stiffness of R/FRC beams depends on the magnitude of tensile stress after crack initiation.

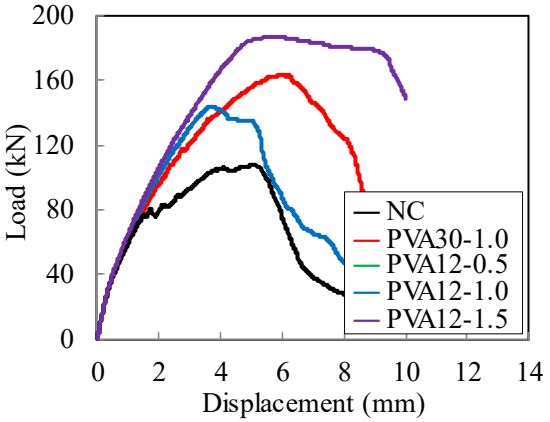

Figure 9: Load-displacement relationships (analysis).

4.2 Shear capacity evaluation via fracture energy

Figure 10 shows the relationship between fracture energy and maximum load for R/FRC beams, as obtained from both experiments and analysis. The fracture energy was calculated based on the fictitious crack width at which the tensile stress becomes zero in the tensile softening curve of each FRC.

From the results of the experiment, it was confirmed that as the fracture energy increased, the maximum load of the R/FRC beams also increased. For PVA30-1.0, the fracture energy was slightly lower than that of PVA12-1.5, however, the maximum load of the R/FRC beam specimens was similar. As mentioned in the previous section, this can be attributed to the rebar yielding of the PVA12-1.5 specimen. The analytical results also indicate that the maximum load tends to increase linearly with the increase in fracture energy. These results reveal that using fracture energy could estimate the shear capacity of R/FRC beams.

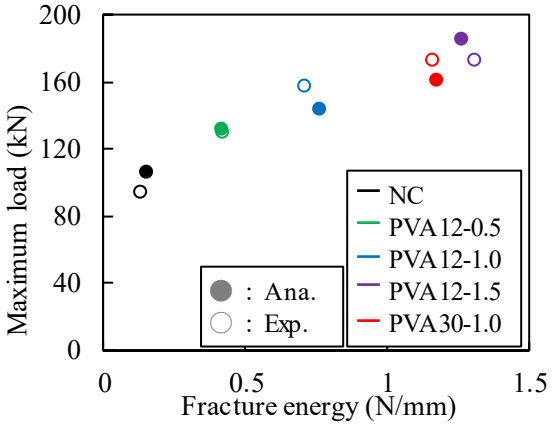

Figure 10: Relationships between fracture energy and maximum load.

5 CONCLUSIONS

This study aimed to clarify the effect of the fiber bridging effect on the shear behavior of FRC members reinforced with steel bars (R/FRC). The shear behavior of these members was evaluated in relation to their tensile softening characteristics. The findings obtained in this study are presented below.

1) FRCs with higher tensile stress in the post-peak region can suppress the opening and propagation of diagonal cracks,

thereby reducing the decrease in stiffness even after diagonal crack formation.

2) Fracture energy exhibits a linear relationship with the shear capacity of R/FRC beams. Therefore, fracture energy can serve as a key parameter for evaluating the shear capacity of R/FRC beams.

REFERENCES

[1] Nakamichi, Y. and Ueda, N., 2020. Fundamental study on material properties of fiber reinforced concrete with micro fiber and its application to reinforced beams subjected to shear loading. *Proc of JCI*. **42(2)**:1063-1068. (in Japanese)

[2] Nakamichi, Y. and Ueda, N., 2021. Study on effect of tension softening properties on bond behavior of reinforced FRC members. *Proc of JCI*. **43(2)**:319-324. (in Japanese)

[3] Japan Concrete Institute, 2003. Method for estimating tensile softening curve of concrete, Appendix (for reference) of the JCI-S-001-2003 (Method of test for fracture energy of concrete by use of notched beam), JCI standard. (in Japanese)

[4] Yamamoto, Y., Nakamura, H., Kuroda, I. and Furuya, N., 2008. Analysis of compression failure of concrete by three dimensional Rigid Body Spring Model. *Doboku Gakkai Ronbunshuu E*. **64(4)**:612-630. (in Japanese)

[5] Niwa, J., Yamada, K., Yokozawa, K. and Okamura, H., 1986. Revaluation of the equation for shear strength of reinforced concrete beams without web reinforcement. *Doboku Gakkai Ronbunshu*, **1986(372)**:167-176. (in Japanese)